УДК 621.039.586 doi.org/10.31717/2311-8253.23.2.5

O. V. Mykhailov, M. V. Saveliev, K. O. Sushchenko, V. V. Dmytryshyn

Institute for Safety Problems of Nuclear Power Plants, NAS of Ukraine, 36a, Kirova st., Chornobyl, 07270, Ukraine

Features of Neutron Flux Density and Gamma-Radiation Exposure Dose Rate Dynamics in ChNPP Shelter Object after the New Safe Confinement Commissioning

Keywords:
Chornobyl NPP,
New Safe Confinement,
Shelter Object,
neutron flux density,
exposure dose rate,
regression analysis,
correlation coefficient

The nuclear safety monitoring system (NSMS), which is a part of the integrated automated monitoring system (IAMS), was created within the framework of measures aimed to build the New Safe Confinement — Shelter Object complex (hereinafter NSC-SO) before the protective arch itself was slide into design position. During NSMS operation period, the attempts were repeatedly made to analyze accumulated measurement data, and a number of important conclusions were obtained regarding the peculiarities of formation of time trends in the dynamics of neutron flux density (NFD) and gamma-radiation exposure dose rate (GDR). To reliably detect any NFD and GDR trends and to predict its further development, special software was developed, deployed and tested at the Institute for Safety Problems of Nuclear Power Plants of the National Academy of Sciences of Ukraine in 2022. The purpose of this work was to summarize the data obtained by special software and to analyze the peculiarities of NFD and GDR dynamics in monitoring point around the nuclear-hazardous clusters of fuel-containing materials (NHC FCM) localized in the NSC-SO, for the period after commissioning of NSC. The research carried out allowed identifying and comparing the general trends in NFD and GDR dynamics, at the same time, for 16 measurement assemblies of NSMS (32 monitoring points located in NSC-SO rooms). It has been established that the control parameters dynamics had two main types according to their manifestation form. The first type is characterized by NFD growth on the background of gradual decrease in the GDR, for the second one — the same character of NFD and GDR changes in the form of simultaneous drop in their mean annual values. Estimated regression equations enabled obtaining quantitative characterization of identified trends regarding NFD/GDR drop or growth and confirmed previously established general trends regarding the behavior of control parameters around the NHC FCM. For majority of monitoring points, gradual GDR drop is noted, but in room 305/2 of NSC-SO, mean annual rate of GDR drop can significantly differ from decay rate of ^{137}Cs radionuclide to the downside. The results obtained in this work allow stating with sufficient confidence that the presence of synchronous NFD growth against the background of synchronous but opposite nature of GDR drop is typical for monitoring points located near the NHC FCM. At the same time, the following phenomenon is typical for monitoring points group, where significant NFD growth is present, and this monitoring area is located in close vicinity to the NHC FCM boundaries: the greater mean annual rate of NFD growth, the slower GDR declines as compared to decay rate of ^{137}Cs radionuclide. The proposed hypothesis is based solely on the results of statistical study of NSMS data and requires further, more in-depth study in order to establish physical nature of the discovered phenomenon.

Introduction

Within the framework of the transformation the Shelter Object into ecologically safe system by the construction of the New Safe Confinement (NSC), and prior to the protective arch was set into design position, an integrated automated monitoring system (IAMS) was created [1]. One of the components of the IAMS is the Nuclear Safety Monitoring System (NSMS), designed for early detection of negative trends that may lead to a reduction in the level of nuclear safety of the NSC-Shelter Object complex (hereinafter referred to as NSC-SO). In automatic mode, NSMS continuously collects, processes, stores, and provides the operational personnel with data on the neutron flux density (NFD) in the energy range from thermal to 1 MeV and the gamma-radiation exposure dose rate (GDR) in the energy range from 0.1 to 4 MeV [2].

During the operation of the IAMS, attempts were made to analyze the accumulated measurement data, and a series of important conclusions regarding the features of temporal trends in the dynamics of NFD and GDR were obtained, however such studies were limited to specific single monitoring points and for curtain monitoring periods only [3–5]. Critical analysis of the obtained data resulted in a conclusion that reliable detection of any behavior trend of any control parameter and forecasting its further development strongly requires a different level of systemic analysis and visualization of numerous measurement data, registered in each measurement channel (MC), front-end processed and filtered by NSMS software [5]. To address this issue, specialized application software (ASW) was developed, deployed, and tested in 2022 on the computing equipment at the Institute for Safety Problems of Nuclear Power Plants of the National Academy of Sciences of Ukraine. The results of testing proved the ability of the developed ASW to perform machine analysis of large volumes of measurement data, determine common trends in the dynamics of NFD and GDR simultaneously for all monitoring points of the IAMS NSMS, and generate reporting materials required for the NSC-SO nuclear safety state assessment.

The purpose of this paper is to summarize the data obtained through IAMS NSMS and the ASW, as well as to perform a detailed analysis of the dynamics of NFD and GDR around nuclear hazardous clusters of fuel-containing materials (NHC FCM) located in the premises of the NSC-SO over the period after the NSC commissioning.

General description of measuring equipment and applied software

The monitoring of GDR and NFD around the zones of FCM clusters in the NSC-SO was conducted using the IAMS NSMS sensor assemblies (SA) containing NDF and GDR detection units (DU) connected to signal processing equipment, which forms so called measurement channels (MC) for NFD and GDR correspondently, the detailed description of which and location of the measurement equipment components within the NSC-SO premises are provided in [2, 5, 7]. Position details (coordinates) of the IAMS NSMS DUs installed inside the boreholes of the NSC-SO in the coordinate system of the ChNPP fourth power unit, are listed in Table 1.

In normal operating mode, MC of SA 01–16 (full identifiers provided in Table 1) are used for measurement; when MC of SA 17–19 (full identifiers also provided in Table 1) are in indicator mode because the control parameter values were at background levels and did not exceed the DU sensitivity threshold.

Technical approaches to processing NSMS data using the developed ASW with descriptions of graphical and tabular materials used as background information for the analysis of GDR and NFD dynamics are detailed in [6]. At this stage of the research, data analysis was conducted within the period of 2018–2022. This is due to the fact that even after the NSC arch was moved into the project position, extensive construction and commissioning works continued on various systems of the NSC-SO. As a result, there were periodic electrical interferences in grounding contours, electronic units were powered off, and adjustments were made to their settings. This led to the measurement data arrays having numerous abnormal results of various origins.

Attempts to statistically process data recorded before 2018 led to the conclusion that quality statistical analysis could only be performed after their full leveling or properly-justified exclusion. However, to achieve this goal, additional filters, not provided in the initial design of the tested ASW version, need to be created. This issue is still relevant and requires resolution in the nearest future.

To assess the degree of clarity of identified trends in each MC and compare them, the values of the relative annual average rate of change for GDR (V_g) and NFD (V_n) were calculated:

$$V_{g(n)} = \frac{1}{4} \times \sum_{i=2018}^{2021} \left(\frac{N_{i+1} - N_i}{N_i}\right) \times 100\%,$$

where N_i i N_{i+1} are the for GDR or NFD average value for the previous or the next year respectively.

Table 1. Location details of GDR and NFD monitoring points of the IAMS NSMS in the NSC-SO complex premises

SA #	MC identifier in operating documents	Monitoring zone	DU center coordinate — monitoring point (axis; line)	Borehole or premises (room)
01	NSMS-S-GDR-001	Room 305/2, +12.0 m	46_{+2850}; $И_{+1400}$	Ю.12.78
	NSMS-S-NFD-001		46_{+2850}; $И_{+1750}$	
02	NSMS-S-GDR-002	Room 305/2, +8.95 m	47_{+800}; $К_{-2000}$	З.9.К
	NSMS-S-NFD-002		47_{+400}; $К_{-2000}$	
03	NSMS-S-GDR-003	Room 305/2, 304/3, +9.3 m	47_{-500}; $И_{-400}$	З.9.Ф
	NSMS-S-NFD-003		47_{-900}; $И_{-400}$	
04	NSMS-S-GRD-004	Room 304/3, +9.85 m	47_{-1000}; $И_{-2000}$	З.10.Г
	NSMS-S-NFD-004		47_{-1400}; $И_{-2000}$	
05	NSMS-S-GDR-005	Room 305/2, +9.1 m	48_{-2450}; $К_{-1000}$	З.9.Ж
	NSMS-S-NFD-005		48_{-2800}; $К_{-1000}$	
06	NSMS-S-GRD-006	Room 305/2, +9.1 m	47_{+700}; К	З.9.68
	NSMS-S-NFD-006		47_{+300}; К	
07	NSMS-S-GDR-007	Room 305/2, +11–11.18 m	49_{-2700}; $И_{+3000}$	З.16.61
	NSMS-S-NFD-007		48_{+3000}; $И_{+3000}$	
08	NSMS-S-GDR-008	SFP*, Room 505/3, +24.6 m	44_{+2950}; $И_{+2200}$	В.21.96
	NSMS-S-NFD-008		44_{+2600}; $И_{+2100}$	
09	NSMS-S-GDR-009	SFP, Room 505/3, +4.0 m	44_{+1700}; $К_{+1000}$	В.4.103
	NSMS-S-NFD-009		44_{+2000}; $К_{+1400}$	
10	NSMS-S-GDR-010	Room 210/6, +6.24–6.32 m	47_{-1800}; $И_{+2050}$	Ю.9.Д
	NSMS-S-NFD-010		47_{-1800}; $И_{+2400}$	
11	NSMS-S-GDR-011	Vault, Room 504/2, +15,0 m	48_{-1700}; $К_{-1000}$	З.15.Д
	NSMS-S-NFD-011		48_{-1300}; $К_{-1000}$	
12	NSMS-S-GDR-012	Vault, Room 504/2, +15,2 m	47_{+900}; $Л_{+2200}$	З.15.В
	NSMS-S-NFD-012		47_{+500}; $Л_{+2200}$	
13	NSMS-S-GDR-013	Room 305/2, +9,1 m	47_{+1200}; $И_{+1650}$	З.9.В
	NSMS-S-NFD-013		47_{+800}; $И_{+1650}$	

Continuation of Table 1

SA #	MC identifier in operating documents	Monitoring zone	DU center coordinate — monitoring point (axis; line)	Borehole or premises (room)
14	NSMS-S-GDR-014	Room 305/2, +9.10 m	47_{-200}; $Л_{-700}$	3.9Ч
	NSMS-S-NFD-014		47_{-600}; $Л_{-700}$	
15	NSMS-S-GDR-015	Room 305/2, 504/2, +14.7 m	48_{-2600}; $К_{+1500}$	3.15.Ж
	NSMS-S-NFD-015		47_{+3000}; $К_{+1500}$	
16	NSMS-S-GDR-016	Room CH**, +32.1 m	48_{-1100}; $И_{+1600}$	3.22.Б
	NSMS-S-NFD-016		48_{-1400}; $И_{+1600}$	
17	NSMS-S-GDR-017	Room under CH, +33.8 m	42_{-1300}; $К_{+1000}$	Room 818/2
	NSMS-S-NFD-017		42_{-900}; $К_{+1000}$	
18	NSMS-S-GDR-018	Room under CH, +33.3 m	42_{-1300}; $К_{+1000}$	Room 818/2
	NSMS-S-NFD-018		42_{-900}; $К_{+1000}$	
19	NSMS-S-GDR-19	Room under CH, +33 m	40_{+500}; $М_{-1500}$	Room 821/2
	NSMS-S-NFD-19		40_{+900}; $М_{-1500}$	

* Southern fuel storage pool, ** Central hall

Discussion and results

Machine data processing with the developed ASW enables to investigate GDR and NFD values dynamics, recorded by the NSMS equipment from 2018 to 2022 (Table 2), assess the features of its trends and determine the regression equations (Table 3).

The coefficient of determination (R^2) values (Table 3) were used as indicators of the goodness-of-fit of the applied model of machine approximation of data (trend) to the initial values of GDR and NFD. Based on the R^2 value defined for each MC, conclusions were made regarding the acceptability of using the obtained regression equation in predicting the behavior of GDR and NFD at the respective NSMS monitoring point in the following years.

Based on the analysis of the obtained data, it was established that the dynamics of GDR and NFD correspond to two main types, which are illustrated in Figs 1 and 2. The first type (see Fig. 1) is characteristic of the opposing trends in the change of control parameters: NFD gradually increases while GDR drops (MC01–07, 10, 12–14, 16). The second type (see Fig. 2) is characteristic of similar consistent changes where both NFD and GDR gradually and simultaneously drop (MC08, 09, 11, 15). In both forms of dynamics, there may be single anomalous results which significantly differ in amplitude, both higher and lower, compared to the predominant number of other results corresponding to a certain general tendency (trend).

The value of R2, estimated for the regression equation of NFD in MC10, 12, 13, 15, and 16, was found to be at a low or very low level (see Table 3), which requires acknowledging the estimated trends as not reliable enough and treat them as indicators of existing tendencies. The results obtained for the monitoring points of NSMS located in room 305/2 fully confirm the data [2–4] regarding the tendency for a gradual increase in NFD near the boundaries of the NHC FCM (see Table 2). At the same time, the regression equations provided in Table 3 made possible a quantitative description of the general trend in the change of GDR and NFD for the entire monitoring zone of NSMS in the premises of the NSC-SO. Comparing the above-mentioned distribution of monitoring points (by the type of dynamics) with the arrangement of MC detection units in the premises of the NSC-SO (see Table 1), the following conclusion can be drawn: in room 305/2, where the NHC FCM is localized or nearby in the adjacent rooms (MC01, 10, 12), GDR and NFD change

Table 2. GDR and NFD year average values for IAMS NSMS monitoring points (m ± std)

SA #	Control parameter	Monitoring period (year)				
		2018	2019	2020	2021	2022*
01	GDR	318.72 ± 1.53	313.42 ± 1.61	307.83 ±1.70	302.23 ± 1.81	297.15 ± 1.39
	NFD	524.69 ± 19.23	534.75 ± 20.10	539.71 ± 19.67	542.66 ± 19.49	548.45 ± 18.66
02	GDR	51.52 ± 0.24	50.71 ± 0.31	49.68 ± 0.29	48.78 ± 0.32	47.88 ± 0.28
	NFD	12.08 ± 0.57	12.82 ± 0.62	13.29 ± 0.63	13.87 ± 0.65	14.37 ± 0.65
03	GDR	25.42 ± 0.09	25.29 ± 0.22	24.62 ± 0.12	24.22 ± 0.17	23.73 ± 0.09
	NFD	63.65 ± 2.84	68.13 ± 2.93	73.54 ± 3.22	78.69 ± 3.13	82.88 ± 3.43
04	GDR	133.83 ± 1.60	129.29 ± 0.94	125.88 ± 0.98	122.83 ± 0.92	119.98 ± 0.75
	NFD	366.71 ± 13.82	369.86 ± 13.60	372.70 ± 8.50	376.78 ± 5.84	383.33 ± 6.13
05	GDR	403.41 ± 2.81	399.75 ± 2.62	386.85 ± 5.55	386.01 ± 0.33	385.00 ± 0.37
	NFD	1515.6 ± 208.6	1976.8 ± 265.3	2519.5 ± 242.6	2734.9 ± 117.7	2654.4 ± 236.1
06	GDR	13.00 ± 0.14	13.03 ± 0.13	12.83 ± 0.09	12.53 ± 0.10	12.22 ± 0.08
	NFD	28.27 ± 1.05	28.99 ± 1.09	32.91 ± 1.47	36.62 ± 1.38	39.42 ± 1.41
07	GDR	1.012 ± 0.017	1.007 ± 0.006	0.992 ± 0.006	0.974 ± 0.006	0.958 ± 0.006
	NFD	95.32 ± 6.58	107.89 ± 5.62	118.58 ± 5.90	129.72 ± 6.32	136.94 ± 5.71
08	GDR	151.39 ± 5.02	145.28 ± 11.44	137.82 ± 8.40	131.22 ± 4.09	124.69 ± 1.92
	NFD	41.96 ± 0.10	41.23 ± 0.86	40.65 ± 0.88	40.08 ± 1.07	39.93 ± 0.87
09	GDR	1964.30 ± 18.75	1910.63 ± 16.71	1866.28 ± 16.29	1812.81 ± 17.40	1774.35 ± 12.44
	NFD	880.81 ± 43.92	865.49 ± 43.15	844.91 ± 44.99	836.40 ± 43.56	840.68 ± 43.76
10	GDR	196.62 ± 1.59	191.33 ± 16.82	180.14 ± 16.76	174.85 ± 6.25	170.50 ± 1.34
	NFD	323.37 ± 14.43	326.54 ± 60.98	332.67 ± 13.15	339.83 ± 12.44	344.88 ± 13.03
11	GDR	70.67 ± 0.77	69.14 ± 0.40	67.74 ± 0.49	66.44 ± 0.40	65.13 ± 0.29
	NFD	86.53 ± 3.01	87.82 ± 2.84	86.29 ± 3.50	84.71 ± 2.93	84.13 ± 2.91
12	GDR	28.58 ± 0.31	27.56 ± 0.16	27.16 ± 0.11	26.70 ± 0.14	26.22 ± 0.10
	NFD	26.44 ± 1.14	26.60 ± 1.01	27.49 ± 2.47	26.77 ± 1.05	26.92 ± 1.04
13	GDR	2.21 ± 0.03	2.19 ± 0.02	2.13 ± 0.02	2.09 ± 0.02	2.04 ± 0.01
	NFD	6.16 ± 0.91	7.11 ± 0.77	7.25 ± 0.50	7.19 ± 0.50	7.23 ± 0.51
14	GDR	22.47 ± 0.17	21.94 ± 0.16	21.31 ± 0.18	20.74 ± 0.16	20.26 ± 0.14
	NFD	116.89 ± 6.08	125.35 ± 6.63	133.85 ± 6.75	141.90 ± 5.93	146.11 ± 5.11
15	GDR	29.61 ± 0.12	29.15 ± 0.13	28.66 ± 0.14	28.21 ± 0.15	27.76 ± 0.11
	NFD	239.86 ± 8.74	239.31 ± 8.30	238.46 ± 8.16	238.51 ± 8.91	236.51 ± 8.27
16	GDR	85.32 ± 0.52	83.40 ± 0.51	81.69 ± 0.52	79.77 ± 0.53	78.12 ± 0.43
	NFD	31.13 ± 3.74	30.96 ± 3.05	32.14 ± 2.24	34.42 ± 2.94	35.23 ± 2.74

Notice. Units of measurement: GDR is measured in Roentgens per hour ($R \cdot h^{-1}$) and NFD is measured in neutrons per square centimeter per second ($n \cdot cm^{-2} \cdot s^{-1}$). The data for 2022 is provided up to the end of November.

Table 3. Results of the regression analysis and assessment of relative annual average rate of change (drop or increase) for GDR and NFD (V_g, V_n)

SA #	Control parameter	Regression equation and coefficient of determination		Relative annual average rate of change for GDR and NFD, %/year	
		Years 2018–2022	R^2	Years 2018–2022	Years 2019–2022
01	GDR	–0.015 x + 321.6	0.998	–1.7	–1.7
	NFD	0.015 x + 524	0.50	1.1	0.9
02	GDR	–0.0026 x + 52.1	0.99	–1.8	–1.9
	NFD	0.0016 x+12	0.95	***4.7***	***4.0***
03	GDR	–0.0012 x +25.6	0.99	–1.7	–2.1
	NFD	0.014 x + 61.3	0.97	***7.6***	***7.2***
04	GDR	–0.0094 x + 134.7	0.99	–2.6	–2.4
	NFD	0.009 x + 366.1	0.51	1.1	1.2
05	GDR	–0.015 x + 406.3	0.84	–1.1	–1.2
	NFD	0.81 x + 1571	0.71	***18.8***	***11.4***
06	GDR	–0.0006 x + 13.2	0.82	–1.5	–2.1
	NFD	0.008 x + 26	0.94	***9.9***	***12.0***
07	GDR	–0.00005 x + 1	0.83	–1.3	–1.6
	NFD	0.028 x + 92.6	0.91	***11.0***	***9.0***
08	GDR	–0.02 x+154	0.66	***–4.4***	***–4.7***
	NFD	–0.0016 x+42.2	0.77	–1.2	–1.1
09	GDR	–0.14 x + 1991.8	0.997	–2.4	–2.4
	NFD	–0.034 x + 882	0.50	–1.1	–1.0
10	GDR	–0.018 x + 196.8	0.40	***–3.3***	***–3.6***
	NFD	0.018 x + 314.1	0.10	1.7	1.9
11	GDR	–0.004 x + 71.2	0.99	–2.0	–1.9
	NFD	–0.002 x + 88.1	0.42	–0.7	–1.4
12	GDR	–0.0016 x + 28.6	0.97	–2.1	–1.6
	NFD	0.0004 x + 26.7	0.02	0.5	0.4
13	GDR	–0.0001 x + 2.3	0.97	–1.9	–2.3
	NFD	0.0005 x + 6.6	0.17	4.3	0.5
14	GDR	–0.0016 x + 22.8	0.999	–2.5	–2.6
	NFD	0.021 x + 114.1	0.98	***6.2***	***5.5***
15	GDR	–0.0013 x + 29.8	0.999	–1.6	–1.6
	NFD	–0.003 x + 241.6	0.15	–0.3	–0.4
16	GDR	–0,005 x + 86,1	0,999	–2,1	–2,1
	NFD	0,0021 x + 31	0,14	3,3	4,6

Notice. Units of measurement: GDR in $R \cdot h^{-1}$; NFD in $n \cdot cm^{-2} \cdot s^{-1}$; x — full day.

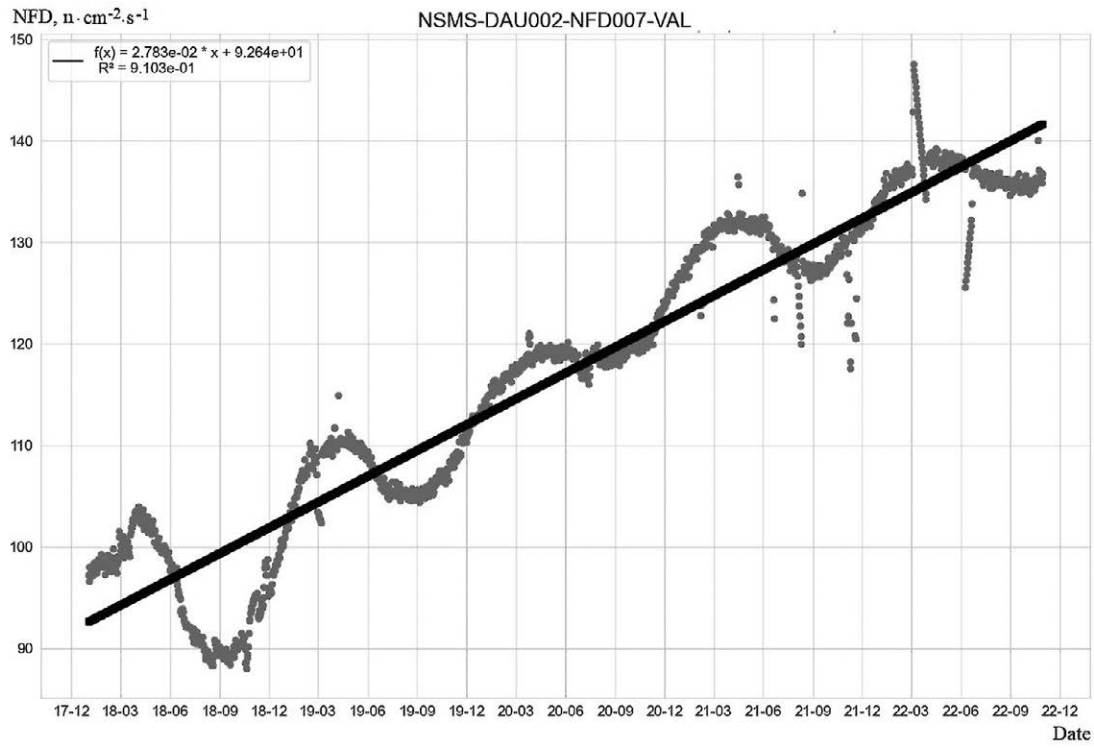

a

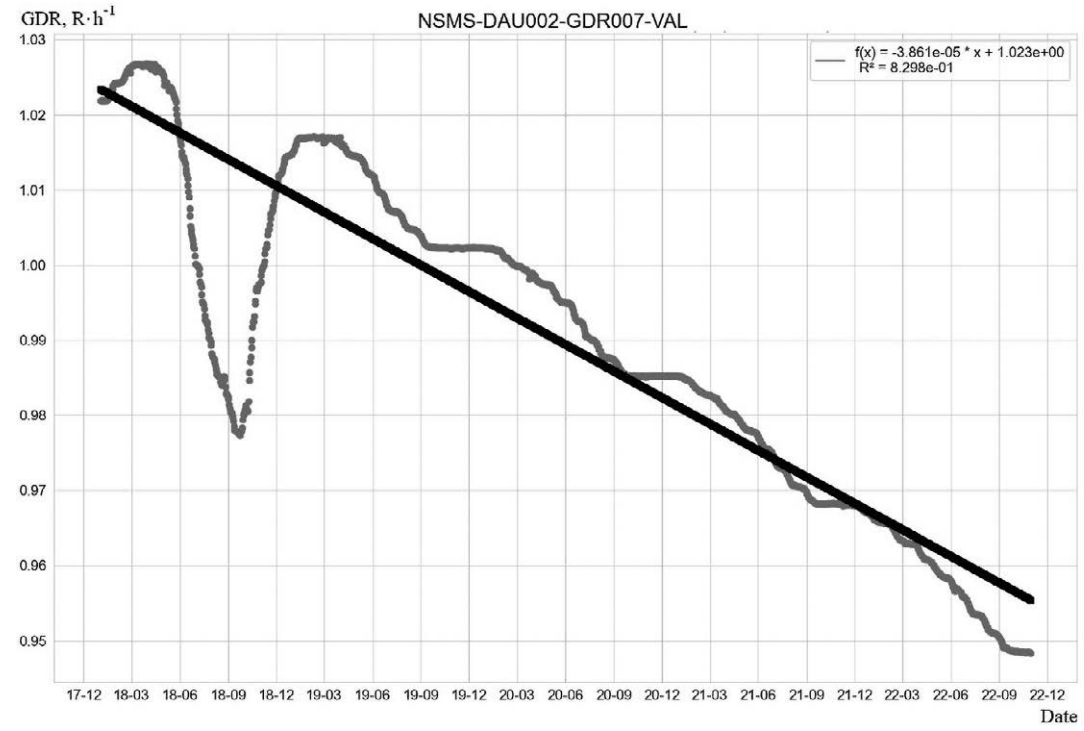

b

Fig. 1. Example of NSMS control parameters values dynamics of the firs type according to the results of machine data processing: a — NFD, b — GDR. Trend graph and regression equation against the background of initial data for SA 07

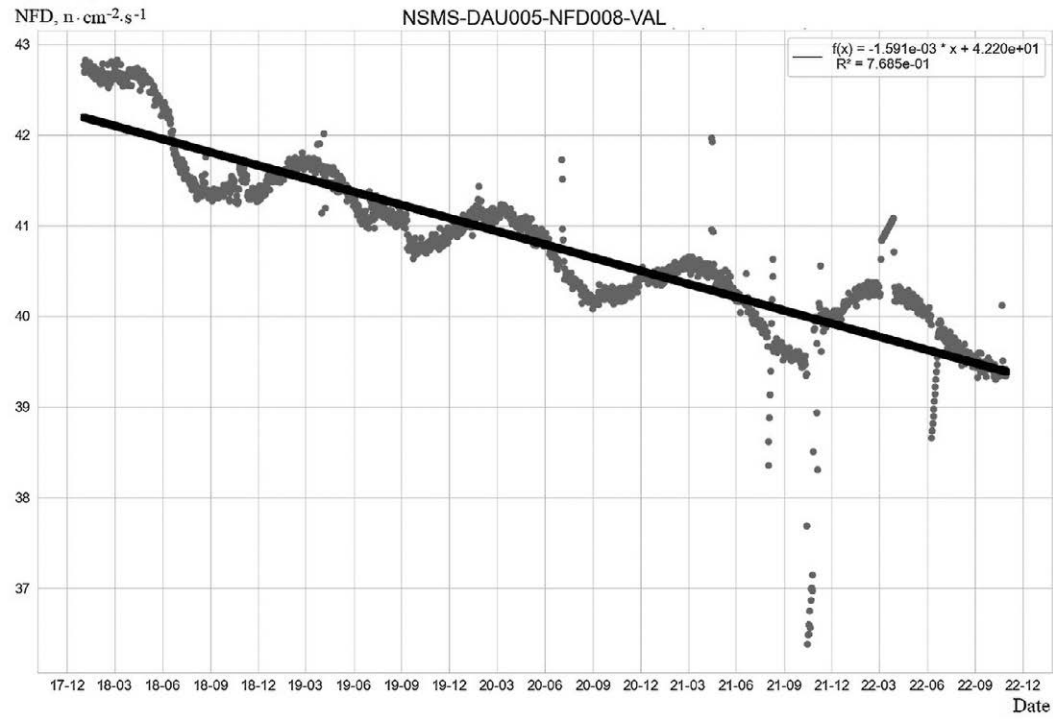

a

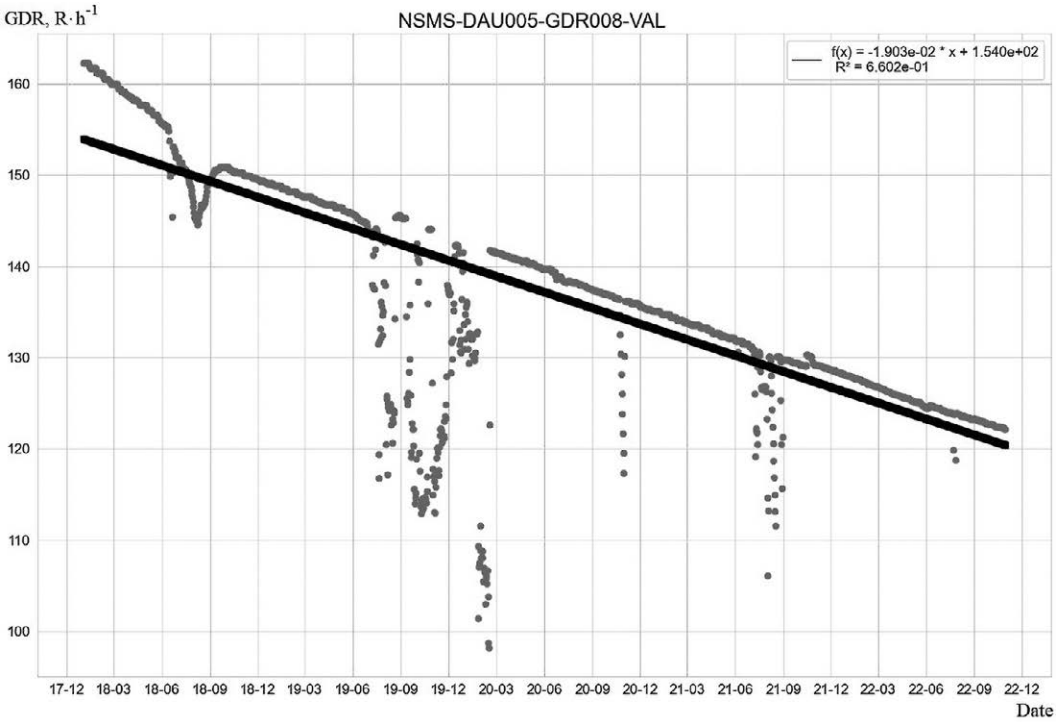

b

Fig. 2. Example of NSMS control parameters values dynamics of the second type according to the results of machine data processing: a — NFD, b — GDR. Trend graph and regression equation against the background of initial data for SA 08

only according to the dynamics of the first type. The dynamics of the second type is not characteristic of this NSMS monitoring zone.

Table 3 shows the calculated results of the relative annual average rates of change in GDR (V_g) and NFD (V_n) for two monitoring periods as of the data presented in Table 2. These calculations were made to assess the reliability of the data under the assumption that since 2019, the impact of construction and commissioning works in the NSC-SO on the operation of the NSMS electronic units was minimized. However, the results of the data comparison presented in Table 3, indicated that the corresponding values of V_g or V_n for both periods did not significantly differ, with the exception of a few V_g values for MC05, 11, and 13. This provided grounds to conclude that the monitoring data for the period 2018–2022 do not contain gross errors accidentally left unfiltered by the ASW and are suitable for further analysis. To estimate the limits of possible ranges of V_g and V_n values, considering the existing discrepancies, the results for both periods were combined, and the following conclusions were drawn. Firstly, NFD is characteristic of both increase ($V_n > 0$) and slightly decrease ($V_n < 0$) over time. Secondly, the gradual increase in NFD observed in most monitoring points can be divided into three intervals by the value of V_n: <1.9 % per year, 4–6.2 % per year, and 7–18.8 % per year. The highest growth rates of NFD (see Table 2) are observed in close proximity to the localization zone of NHC FCM in room 305/2. Thirdly, the opposite trend of slight NFD decrease ($|V_n| < 1.4$ % per year) is found only for a few monitoring points, including MC08 and 09, whose detection units are located near the southern fuel storage pool (see Table 1). At the same time, for the NSMS monitoring zone near the southern fuel storage pool the NFD decreasing trend is constant and reliable (see Table 2, regression equations for MC08 and 09). Fourthly, unlike NFD, GDR is characteristic of a persistent decrease trend only (see examples in Figs 1.b and 2.b) and all MC can be grouped into three intervals of V_g values, %/year: <1.3, 1.6–2.6, and 3.3–4.7. Moreover, for the monitoring points located near the boundaries of NHC FCM in room 305/2 (MC01–03, 05–07, 13, and 14), the average value of V_g is –1.7 % per year, which is 1.4 times less than the decay rate of the ^{137}Cs radionuclide (V_{Cs} = –2.28 % per year), based on the half-life of ^{137}Cs (30.1 years). In this case, ^{137}Cs was used as a stable marker, the law of radioactive decay of ^{137}Cs provides a sort of checkpoint against which the values of V_g calculated for different monitoring points were compared. As can be seen from Table 3, the highest V_g value is observed in MC08 located near the southern fuel storage pool. At the same time, in MC09, V_g almost coincides with V_{Cs}.

Another important aspect explored in the study is worth noting. Figs 3 and 4 present the results of the search for correlations between weekly average values of NSMS control parameters in different MC. The chosen method of presenting the report information in the form of pairwise correlation coefficients (CC) matrix allowed obtaining an integral characteristic of the degree of connection between GDR values (see Fig. 3) or NFD values (see Fig. 4) simultaneously for all monitored rooms of the NSC-SO for the monitoring period.

As seen in Fig. 3, the results of the regression analysis demonstrate a common trend from 2018 to 2022 for synchronous change (decrease) in GDR in all the rooms of the NSC-SO monitored by NSMS, with one exception (MC03). In contrast to GDR, the relationships pattern for NFD was not as consistent. However, based on the analysis of CC values, it is possible to clearly distinguish MC for which synchronous increase in NFD values is representative. First, this is a group of MCs with detector units installed near the localization zone of NHC FCM (with the exception of MC 13). Second, synchronous increase in NFD is observed not only within the abovementioned group of MC but also concurrently with the other MCs, whose detector units are installed at different elevation marks within the NSC-SO outside the room 305/2.

Therefore, the results presented above allow for a fairly confident assertion that NSMS monitoring points located near the NHC FCM exhibit synchronous increase in NFD. At the same time, the dynamics of GDR within this zone also have synchronous but opposite pattern. Detailed analysis of the revealed GRD and NFD dynamics features in NSMS monitoring points with annually recorded constant and significant increase in NFD shows that the value of V_g may be significantly lower than V_{Cs} (Fig. 5.a).

For a clearer understanding of the phenomenon not observed before, the monitoring points, where significant NFD growth ($V_n < 1.2$ % per year) and the effect of V_g decline rate slowdown compared to V_{Cs} ($|V_g| \geq |V_{Cs}|$) were not detected, were excluded from the data sample depicted in Fig. 5.a. As seen, the regression analysis results represented in Fig. 5.b, hardly differ in terms of the functional dependence between V_g and V_n. Moreover, the approximating function in Fig. 5.b has high reliability (CC = 0.96 for R2 = 0.92). In Fig. 6, the results depicted in Fig. 5.b are presented in a slightly different form, showing the functional dependence of the absolute difference between V_{Cs} and V_g($A_v = V_{Cs} - V_n$) on the value of V_n. This representation provides a more visual demonstration of how the GDR decline rate slowdown compared to the decay rate of ^{137}Cs depends on the value of V_n, i. e., on the NFD increase. As mentioned earlier, this phenome-

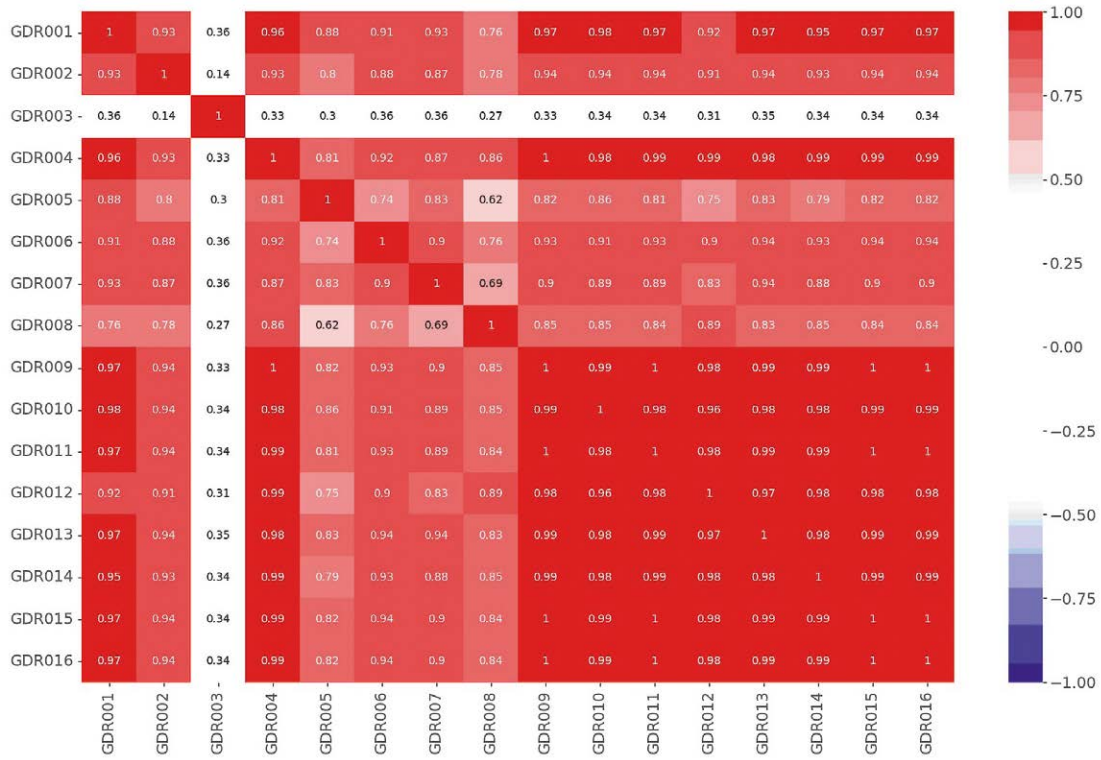

Fig. 3. Results of the NSMS data machine processing in the form of the pair CC matrix for weekly average GDR values in different MC (2018–2022 years)

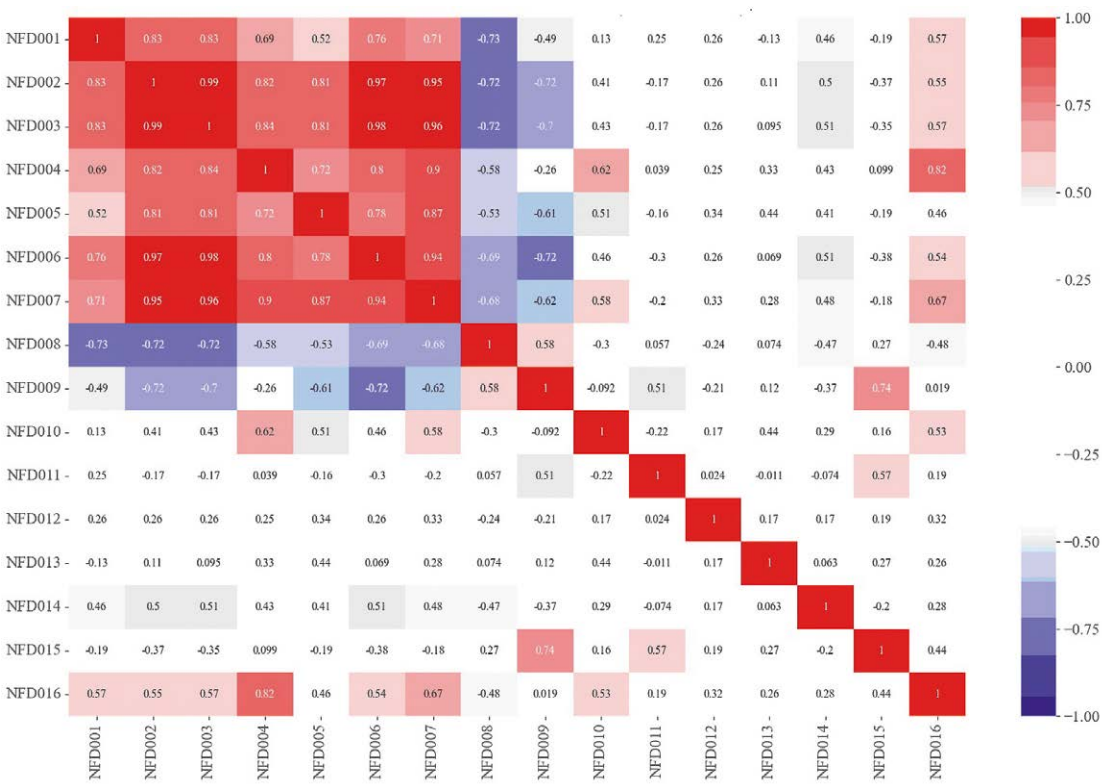

Fig. 4. Results of the NSMS data machine processing in the form of the pair CC matrix for weekly average NFD values in different MC (2018–2022 years)

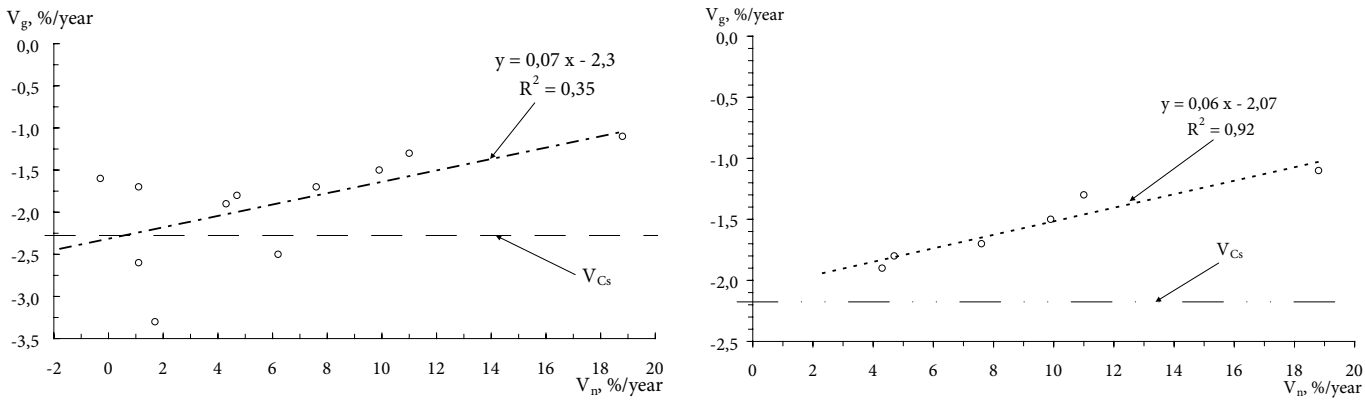

Fig. 5. Functional dependence between the rate of change in GDR and NFD: a — all the monitoring points are located near the boundaries of NHC FCM; b — monitoring points, where significant increase of NFD is observed

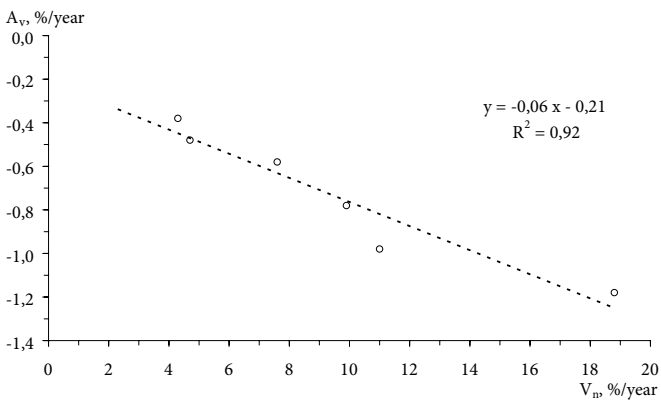

Fig. 6. The GDR decline rate slowdown compared to the decay rate of ^{137}Cs (A_v) dependent on the NFD (V_n) increase rate around the NHC FCM localization

non has not been observed before the NSC commissioning. Based on the data obtained for 2018–2022, there is no reason to believe that it may be characteristic of other areas within the NSC-SO. Therefore, it can be assumed that this phenomenon is specific to the NSMS monitoring zone around the boundaries of the NHC FCM localization.

Conclusions

The research conducted within this study made possible the determination and comparison of the general trends in GDR and NFD dynamics after the commissioning of the NSC. These trends were observed simultaneously for 16 measurement channels of the NSMS IAMS, with detection units located in different areas and at various elevation marks of the NSC-SO. Taking into account the latest data, it can be confidently stated that the dynamics of GDR and NFD can be categorized into two main types. The first type features an increase in NFD alongside a gradual decrease in GDR, while the second type presents a similar change pattern for GDR and NFD, showing a simultaneous reduction in their average annual values.

The defined regression equations allowed for a quantitative description of the observed trends in GDR and NFD changes around the NHC FCM. A gradual decrease of GDR is observed in the NSC-SO. However, in the monitoring points in room 305/2, where significant annual increases in NFD are recorded, the dynamics of GDR, in terms of the decline rate, may be slower compared to the decay rate of the radionuclide ^{137}Cs: the greater mean annual rate of NFD growth in this monitoring zone, the slower GDR declines as compared to decay rate of ^{137}Cs radionuclide. The hypothesis put forward is solely based on the results of the statistical analysis of the NSMS data obtained from 2018 to 2022. It requires further in-depth investigation to determine the physical nature of the observed phenomenon.

References

1. Krasnov V. O., Nosovskyi A. V., Paskevych S. A., Rudko V. M.; A. V. Nosovskyi (ed.) (2021). *Obiekt "Ukryttia" v umovakh novoho bezpechnoho konfainmenta* [The Shelter Object in Conditions of the New Safe Confinement]. Chornobyl: ISP NPP, NAS of Ukraine, 344 p. (in Ukr.)
2. Saveliev M. V., Godun R. L., Pantin M. A., Skiter I. S., Sushchenko K. O. (2022). The nuclear safety monitoring system for fuel-containing materials located in destroyed Unit No. 4 of the Chornobyl NPP and proposals for its modernization. *Nuclear Physics and Atomic Energy*, vol. 23, pp. 172–181.
3. Vysotskyi Ye. D., Godun R. L., Doroshenko A. O. (2018). [The dynamics of neutron activity and subcriticality level

of a nuclear-dangerous cluster in the conditions of NSC-SO complex]. *Problems of Nuclear Power Plants Safety and of Chornobyl*, vol. 30, pp. 78–86. (in Rus.)
4. Pavliuchenko M. I., Krasnov V. A. (2018). [Brief analysis of results of measured neutron flux density and gamma dose rate in borehole Ю.12.78 of the Shelter object]. *Problems of Nuclear Power Plants Safety and of Chornobyl*, vol. 31, pp. 104–108. (in Ukr.)
5. Vysotskyi Ye. D., Sushchenko K. O., Godun R. L. (2020). [Expert assessment of the current criticality level of clusters of fuel-containing materials after the New Safe Confinement installing]. *Nuclear Power and the Environment*, vol. 1 (16), pp. 49–56. (in Rus.)
6. Saveliev M. V., Mykhailov O. V., Sushchenko D. O. (2022). [Machine analysis of exposure dose rate and neutron flux density dynamics in the Shelter object according to the data from the nuclear safety monitoring system]. *Nuclear Power and the Environment*, vol. 3 (25), pp. 24–32. (in Ukr.)
7. *IAMS-OVER-ZS-1103-E. Technical Design*. Explanatory Note, 2005.

О. В. Михайлов, М. В. Савельєв, К. О. Сущенко, В. В. Дмитришин

Інститут проблем безпеки АЕС НАН України, вул. Кірова, 36а, Чорнобиль, 07270, Україна

Особливості динаміки щільності потоку нейтронів та потужності експозиційної дози γ-випромінювання в об'єкті «Укриття» Чорнобильської АЕС після введення нового безпечного конфайнмента в експлуатацію

Проведено аналіз даних системи контролю ядерної безпеки інтегрованої автоматизованої системи контролю (СКЯБ ІАСК) та досліджено загальні тенденції зміни щільності потоку нейтронів (ЩПН) та потужності експозиційної дози (ПЕД) γ-випромінювання у приміщеннях об'єкта «Укриття» (ОУ) після введення комплексу нового безпечного конфайнмента (НБК-ОУ) в експлуатацію. Зроблено висновки щодо особливостей формування динаміки ЩПН та ПЕД у різних точках контролю СКЯБ ІАСК навколо ядерно-небезпечних скупчень паливовмісних матеріалів (ЯНС ПВМ), локалізованих у приміщенні 305/2 комплексу НБК-ОУ. Визначені тренди зміни параметрів контролю СКЯБ описано за допомогою рівнянь регресії. Проведено порівняння середньорічної швидкості зменшення ПЕД у різних приміщеннях комплексу НБК-ОУ зі швидкістю розпаду радіонукліда ^{137}Cs. Визначено, що у точках контролю СКЯБ, де щороку після введення в експлуатацію НБК реєструється значне зростання ЩПН, одночасно спостерігається суттєве уповільнення середньорічної швидкості зменшення ПЕД порівняно зі швидкістю радіоактивного розпаду ізотопу ^{137}Cs. Запропоновано рівняння регресії, яке кількісно пов'язує уповільнення зменшення ПЕД залежно від збільшення ЩПН у точках контролю СКЯБ ІАСК навколо зони локалізації ЯНС ПВМ.

Ключові слова: Чорнобильська АЕС, новий безпечний конфайнмент, об'єкт «Укриття», щільність потоку нейтронів, потужність експозиційної дози, регресійний аналіз, коефіцієнт кореляції.

Надійшла 16.03.2023
Received 16.03.2023